ELSEVIER

Journal of Nuclear Materials 241–243 (1997) 618–622

journal of nuclear materials

Impurity feedback control for enhanced divertor and edge radiation in DIII-D discharges

G.L. Jackson [a,*], G.M. Staebler [a], S.L. Allen [b], N.H. Brooks [a], T.E. Evans [a], J.R. Ferron [a], A.W. Leonard [a], R. Maingi [c], T.W. Petrie [a], M.J. Schaffer [a], R.D. Wood [b], W.P. West [a], D.G. Whyte [d]

[a] *General Atomics, P.O. Box 85608, San Diego, CA 923186-9784, USA*
[b] *Lawrence Livermore National Laboratory, Livermore, CA, USA*
[c] *Oak Ridge Associated Universities, Oak Ridge, TN, USA*
[d] *INRS, Energie et Materiaux, Varennes, Que., Canada*

Abstract

Radiated power fractions above 90% have been achieved in DIII-D using impurity feedback control. Heat flux reductions up to a factor of 6 and confinement enhancements of $1.6 \times$ ITER-89P L-mode scaling have been obtained with a radiated power fraction above 90%. When the outer separatrix strike point was positioned for pumping with the DIII-D cryopump, ELMing H-mode (Type III ELMs) was triggered with neon feedback injection in conjunction with a constant deuterium gas puff rate. Changes in the ELM frequency, energy confinement and central neon concentrations as a function of radiated power are presented. Observations of detached discharges with H-mode confinement similar to the ASDEX-U CDH-mode are also discussed.

Keywords: DIII-D; poloidal divertor; radiation energy sink

1. Introduction

Long pulse and steady state fusion ignition devices will require a significant radiated power fraction to minimize heat flux to, and sputtering of, the first wall. While impurity gases have been proposed to enhance radiation, precise control of impurity gas injection is essential to achieve an adequate radiative power fraction while maintaining good energy confinement and low central impurity concentration. We report here the first experiments in the DIII-D tokamak using feedback control of the rate of impurity gas injection. These experiments were carried out with active divertor pumping using the in-situ DIII-D cryopump. The radiated power fraction was controlled by sensing either UV edge line radiation (Ne^{+7}) or mantle radiation from selected bolometer channels and using the DIII-D digital plasma control system to calculate radiated power real-time and generate an error signal to control an impurity gas injector valve.

Impurity radiation has been used on other devices to obtain low heat flux to plasma facing surfaces while maintaining good energy and particle confinement in the plasma core without excessive impurity contamination. The TEXTOR tokamak has used siliconization and neon gas puffing to obtain a highly radiative mantle while maintaining energy confinement significantly above the ITER 89P L-mode empirical scaling relation [1,2]. More recently, the ASDEX-U tokamak has demonstrated H-mode confinement in a diverted discharge under completely detached conditions (CDH-mode).

In this paper we present the implementation of a feedback control method which uses either bolometer signals or UV impurity line radiation to control the fueling rate of a main chamber neon injector. Using this hardware, we have successfully controlled the fraction of radiated power and obtained energy confinement above ITER-89P L-mode

* Corresponding author. Tel.: +1-619 455 2157; fax: +1-619 455 4156; e-mail: jackson@gav.gat.com.

PII S0022-3115(96)00575-2

scaling for radiated power fractions, P_{fr}, $\gtrsim 90\%$. Transient phases of the CDH-mode have been observed with energy confinement enhancements, $\tau_E/\tau_{ITER\text{-}89P} \leq 1.6$. In this paper we define the fraction of radiated power, $P_{fr} = P_{rad}/(P_{tot} - dW_{MHD}/dt)$, where P_{rad} is the total radiated power including divertor radiation measured by a 48 channel bolometer system, P_{tot} is the total input power from neutral beam injection and Ohmic heating and W_{MHD} is the plasma stored energy.

2. The DIII-D impurity feedback control system

For the discharges reported here, the fraction of radiated power during the H-mode phase is determined by gas puffing both deuterium (fixed puff) and neon (feedback control) from a location above the midplane. The discharge shape is single null lower divertor with the ∇B ion drift direction towards the X-point. The experimental geometry is shown in Fig. 1. The divertor strike point is positioned near the entrance of the pumping plenum which contains a toroidally continuous liquid helium cryopump for active pumping. The location of divertor diagnostics discussed later in the paper is also shown in Fig. 1.

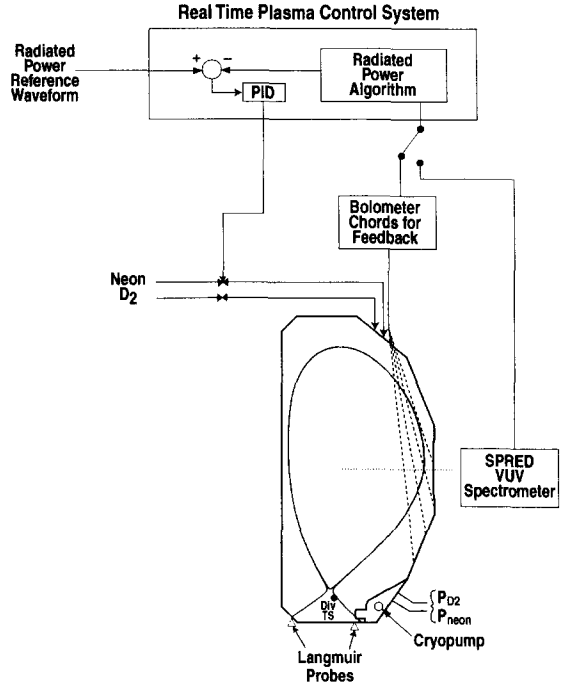

Fig. 1. DIII-D geometry for active impurity feedback control. The separatrix flux surface is shown as a solid line. The outer strike point defined by this flux surface is positioned for pumping with the toroidally symmetric cryopump. Radiated power is calculated using either four channels of the bolometer array or a Ne^{+7} UV impurity line. Not all channels of profile diagnostics are shown; only the locations of key diagnostics discussed in this paper are indicated.

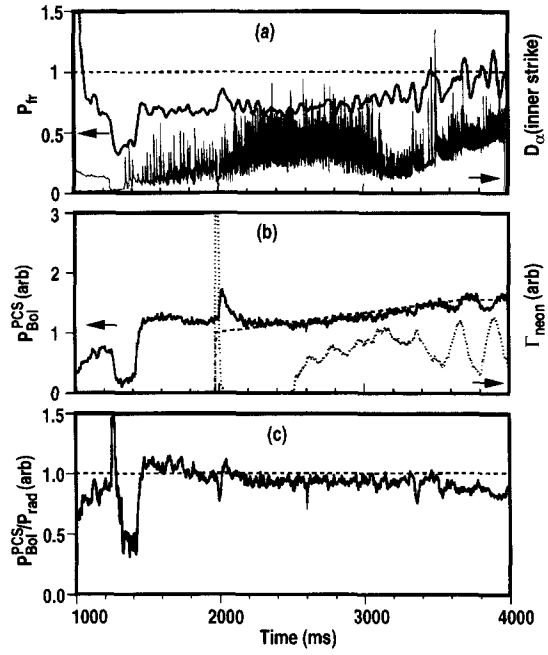

Fig. 2. P_{fr} is controlled by puffing neon during a tokamak discharge (#86947, $I_p = 1.3$ MA, $B_t = 1.9$ T, $P_{NBI} = 6.3$ MW). The reference waveform (dashed line) and four channel bolometer radiated power, P_{Bol}^{PCS}, are compared in (b). Neon gas puffing rate, Γ_{neon}, is also shown. The ratio of total radiated power, P_{rad}, to calculated power used by the digital PCS is shown in (c).

Feedback control is achieved by using the DIII-D digital plasma control system (PCS) to calculate radiated power in real time using four bolometer channels [3]. An alternative algorithm estimates radiated power using Ne^{+7} (77 nm) line emissivity measured by the SPRED spectrometer. Either calculation is compared with a reference waveform for radiated power and the error signal is used for feedback control of the neon gas input rate, shown schematically in Fig. 1. Proportional, integral and derivative gain (PID) can be optimized by changing parameters in the PCS on a shot-by-shot basis [3].

Data from a discharge in which radiated power was controlled using bolometer signals is shown in Fig. 2. In this case, the reference radiated power was monotonically increasing from 2.0 to 3.7 s. Although feedback control had not been optimized, measured bolometer power calculated by the PCS (Fig. 2(b)) approximates the reference waveform. Note that during the H-mode phase when impurity feedback control was enabled, 2.0 to 3.5 s, the ratio of PCS radiated power calculated in real time to total radiated power from the entire bolometer array was nearly constant (Fig. 2(c)), which allowed feedback control of P_{fr}.

3. Plasma discharges with active feedback control

In order to test the DIII-D active impurity feedback system, a series of discharges was initiated, varying both the deuterium and neon gas puff rates. Since the primary goal was to qualify the feedback system, there was no attempt to obtain feedback control at a constant P_{fr} for long durations. An example of active impurity feedback control is shown in Fig. 3. Neutral beam power, $P_{NBI} = 6.3$ MW, was constant during the time shown. A constant deuterium puff, at 180 T L/s was initiated at 1.4 s. The outer strike point was positioned at the entrance of the cryopump plenum. Impurity feedback control, using the Ne^{+7} impurity line radiation, was initiated at 2.0 s. Radiated power increased, in response to the programmed waveform until $P_{fr} \approx 1$ at 3.2 s, shown in Fig. 3(b). Shortly after the radiated power exceeded the input power, at $t = 3.3$ s in Fig. 3(a), the discharge transitioned back to L-mode. ELM behavior during H-mode is plotted in Fig. 3(a). After a short ELM free phase, type I large amplitude ELMs [4] begin and continue after deuterium injection begins at 1.4 s. After neon injection commences at 2.0 s, combination ELMs (type I and type III) are observed. Finally, when P_{fr} reaches approximately 0.9 there is a brief transition back to L-mode (2.9 s in Fig. 3) and then type III ELMs are observed. The uncertainty in total radiated power and P_{fr} is estimated to be 10–15%. This is higher than usual due to gas puffing from a toroidal location near the upper bolometer array. The behavior of divertor heat flux measured by an IRTV camera, for which data is plotted in Fig. 3(c), also evolves and decreases during the various phases of gas puffing. During part of the discharge the outer strike point was at the entrance to the cryopump which is not in the field of view of the IRTV. Hence, only inner strike point peak heat flux is plotted in Fig. 3(c). During neon impurity injection, peak heat flux remains low including the phase with type III ELMs. Central Z_{eff}, determined from impurity concentrations of neon, carbon, oxygen and helium and measured by charge exchange recombination radiation in the VUV, increases slightly after neon injection at 2.0 s, then increases further with the onset of type III ELMs. The change from a combination of type I and type III ELMs ($t < 2.9$ s in Fig. 3) to only type III ELMs does produce an increase in central neon concentration, the dominant core

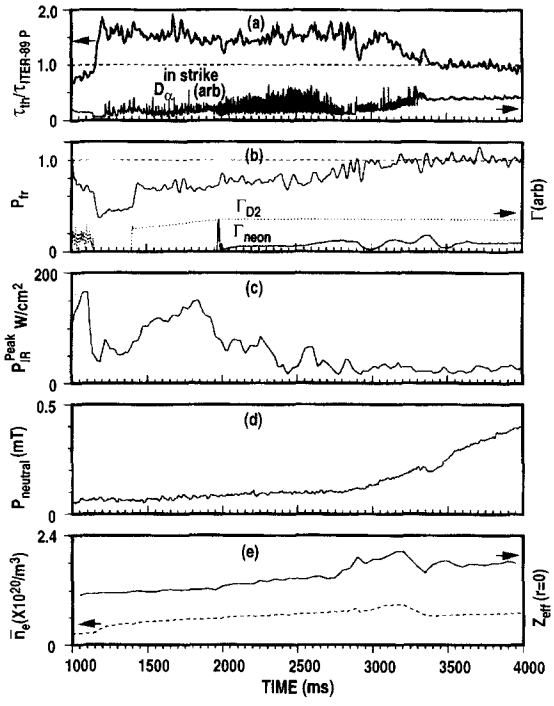

Fig. 3. H-mode confinement is up to 1.6×ITER89-P during ELMing H-mode, (a), in phases of deuterium (Γ_{D2}) and neon (Γ_{neon}) puffing with $P_{fr} \leq 1$, (b). Peak power, P_{IR}^{Peak}, is measured by IRTV, (c), for the inner strike point. Neutral pressure in the main chamber increases during type III ELMs and L-mode (d). Central Z_{eff} (not absolutely calibrated) and line average density are plotted in (e). Discharge parameters (#86948) are the same as in Fig. 2. This discharge used neon feedback from a Ne^{+7} line.

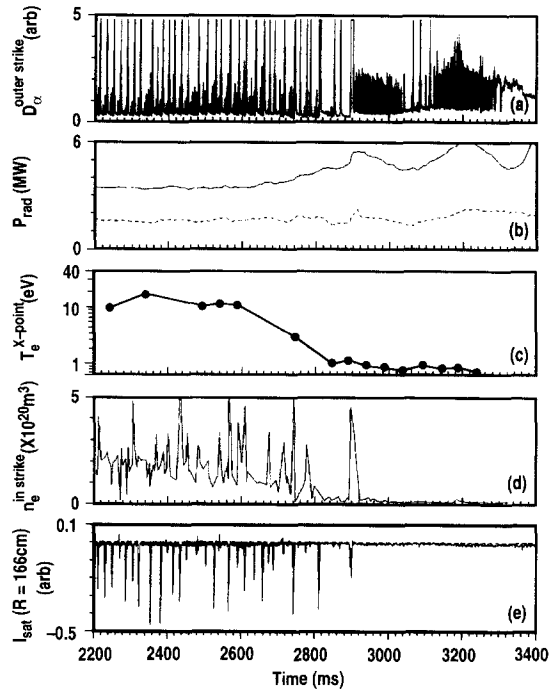

Fig. 4. Same discharge as in Fig. 3, showing the phase with neon puffing: (a) D_α at the outer strike point, (b) radiated power from the mantle (solid line) and divertor (dashed), (c) electron temperature near the X-point, (d) electron density at the inner strike point calculated from a floor Langmuir probe and (e) current from a floor Langmuir probe at $R = 166$ cm, inside of, but near the outer strike point.

impurity and hence an increase in Z_{eff}. The value of Z_{eff} in Fig. 3(c) is not absolute because a complete calibration of central impurity densities is still in progress. Finally, we note that after 2.9 s, neutral pressure in the main chamber increases monotonically, as shown in Fig. 3(d).

The change to type III ELMs at 2905 ms, preceded by a brief L-mode confinement phase and subsequent low conducted heat to the divertor tiles has characteristics similar to CDH-mode reported recently on the ASDEX-Upgrade device [5,6]. This phase is shown in more detail in Fig. 4 for the same discharge as Fig. 3. After 2.9 s, the increase in radiated power, Fig. 4(a), is from the main chamber. Bolometric profiles during this phase confirm that the increased radiation is not from the divertor, but rather from a radiating mantle around the plasma core. At 2950 ms, 3.4 MW is radiated from inside the last closed flux surface (LCFS) excluding the region near the X-point. Before the onset of continuous type III ELMs, which occurs at 2905 ms in Figs. 3 and 4, there is a gradual evolution of divertor parameters, e.g. Fig. 4(c–e). Electron temperature, measured by divertor Thomson scattering near the X-point (location is shown in Fig. 1), decreases to < 2 eV at 2800 ms, while electron density (not shown) increases by more than a factor of 2 to $\approx 1 \times 10^{20}/m^3$. Electron density at the inner strike point, measured by a floor Langmuir probe (Fig. 1), steadily decreases from 2.2 to 2.9 s. Although accurate fits of Langmuir probe data to obtain temperature and density were not possible near the outer strike point, the probe saturation current, shown in Fig. 4(e), shows no evidence of ELMs penetrating to the floor probe nearest the outer strike point after 2.9 s. During this phase there is no evidence of these spikes on any Langmuir probe in the floor array, including those at the inner strike point. The Langmuir probe voltage is swept at 250 Hz and before 2.9 s in Fig. 4(e) large amplitude spikes are present if the sweep voltage is biased negative during the type I ELMs i.e. density at the floor increases during these ELMs. These observations are consistent with detachment of the plasma from 2.9 to 3.3 s in the divertor region while maintaining H-mode confinement. We note that during this period, the H-factor (Fig. 3(a)) varied from 1.2 to 1.6, and was actually increasing during the first period of type III ELMs. Although not shown in Fig. 3, an H-factor of 1.6 is equivalent to JET-DIII-D empirical confinement scaling for these discharges i.e. $\tau_E/\tau_{JET\text{-}DIII\text{-}D} = 1.0$ for $H = 1.6$.

4. Discussion

Active impurity feedback using neon has been successfully demonstrated using either bolometer channels or a neon UV impurity line to control the fraction of radiated power. Although not fully optimized, the DIII-D digital plasma control system has demonstrated the capability of rapid feedback control under evolving conditions such as changing ELM frequency.

The observations of detachment, shown in Fig. 4 and presented in Section 3, are consistent with the CDH-mode observed in ASDEX-U. In this initial one day experiment, only short CDH-mode phases were observed in DIII-D. This was because P_{fr} was programmed to monotonically increase during the discharges, e.g. Fig. 2, to rapidly cover parameter space. Hence the radiation limit, $P_{fr} = 1$, was reached shortly after the CDH-mode was established and the discharge reverted to L-mode confinement. A further reason that the CDH-mode phase may have terminated early was that the main chamber neutral pressure began increasing after detachment. This may be caused by a decrease in pumping efficiency, since thermalized neutral particles are the primary constituents at the cryopump pump inlet after detachment. Future experiments will focus on maintaining high radiated power ($P_{fr} > 0.8$) in steady state conditions.

Radiation inside the LCFS during the initial CDH-mode phase in Fig. 4 was 3.4 MW, or 45% of the input power, P_{tot}. The power crossing the LCFS is then estimated to be 4.1 MW, which is significantly higher than the threshold power for the L to H transition which is estimated from empirical scaling to be $\lesssim 2$ MW [7]. We note, however that due to the effects of gas puffing near the upper bolometer array viewing port, the contribution of radiated power in the X-point region which was inside the LCFS could not be measured and this power was excluded from the calculation. The contribution of this radiated power would decrease the power flowing across the LCFS to a value closer to the L to H threshold power as observed on ASDEX-U CDH-mode discharges [5,6].

Although one discharge has been discussed in detail, similar behavior was observed on other discharges. The time of the H to CDH transition varied depending upon the rate of rise of programmed radiated power, however this transition is only observed if $P_{fr} \gtrsim 0.9$. We note that these discharges exhibited q profiles which had weak negative central shear (NCS) [8] and $q_{min} > 1$. Whether NCS is necessary to obtain the CDH-mode will require further experiments.

Particle confinement time is an important issue for fusion reactors: hydrogenic particles must have sufficient time to react while impurity confinement time must be low to avoid central accumulation. Particle confinement is difficult to measure directly in devices such as DIII-D with a divertor configuration and a discussion of particle confinement is beyond the scope of this paper. Previous work in DIII-D has shown that the ELM free global particle confinement time is of the same order as the energy confinement time [9,10]. Changes in particle confinement time during ELMing CDH-mode have not yet been measured or calculated.

Future work in the area of active impurity feedback control will include: the use of different impurity gases, steady state CDH-mode, other high P_{fr} regimes such as TEXTOR L-mode enhanced confinement discharges, a

better algorithm for calculating P_{fr} in the mantle and optimization of energy confinement while maintaining $Z_{eff} < 2$.

Acknowledgements

Work supported by U.S. Department of Energy under Contract No's. DE-AC03-89ER51114, W-7405-ENG-48 and DE-AC05-96OR22464.

References

[1] J. Winter, H.G. Esser, G.L. Jackson et al., Phys. Rev Lett. 71 (1993) 1549.
[2] J. Ongena et al., Plasma Phys. Controlled Fusion 83 (1996) 279.
[3] M. Walker, J.R. Ferron, B. Penaflor et al., Proc. 16th IEEE/NPS Symp. on Fusion Engr., Champagne, IL, USA (1995).
[4] E.J. Doyle et al., Phys. Fluids B 3 (1991) 2300.
[5] O. Gruber, A. Kallenbach, M. Kaufmann et al., Phys. Rev. Lett. 74 (1995) 4217.
[6] A. Kallenbach, R. Dux, V. Mertens et al., Nucl. Fusion 35 (1995) 1231.
[7] ITER Working Group on Confinement Databases and Modeling, Bull Am. Phys. Soc. 40 (1995) 1726.
[8] E.A. Lazarus, G. Navratil, C.M. Greenfield et al., Nucl. Fusion (1996), accepted for publication.
[9] G.L. Jackson, D.R. Baker, K.L. Holtrop et al., J. Nucl. Mater. 220–222 (1995) 173.
[10] L.W. Owen, R. Maingi, D.K. Lee et al., J. Nucl. Mater. 220–222 (1995) 315.